

High-resolution mapping of iso-orientation columns by fMRI

Dae-Shik Kim, Timothy Q. Duong and Seong-Gi Kim

Center for Magnetic Resonance Research, University of Minnesota Medical School, 2021 6th Street S.E., Minneapolis, Minnesota 55455, USA
Correspondence should be addressed to S.-G.K. (kim@cmrr.umn.edu)

Blood-oxygenation level-dependent (BOLD) functional magnetic resonance imaging (fMRI) is an important tool for localizing brain functions *in vivo*. However, the ability of BOLD fMRI to map cortical columnar structures is highly controversial, as the ultimate functional specificity of BOLD remains unknown. Here we report a biphasic BOLD response to visual stimulation in the primary visual cortex of cats. In functional imaging, the initial BOLD signal decrease accurately labeled individual iso-orientation columns. In contrast, the delayed positive BOLD changes indicated the pattern of overall activation in the visual cortex, but were less suited to discriminate active from inactive columns.

Localization is a principle that is widely used in brain: cytoarchitecturally distinct areas form the basis for functional specialization¹. Such parcellation of the cortical tissue into functional subunits is especially prominent at the level of individual cortical columns. In visual cortex of mammals, neurons with similar response properties such as ocular dominance or orientation preference are clustered into columns, spanning the entire cortical plate from the pia to white matter^{2–4}. Studies of the structure, function and plasticity of cortical columns using a variety of traditional mapping techniques, however, suffer from fundamental limitations. For example, intra- and extracellular recordings yield insufficient field of view, and the 2-deoxyglucose⁵ technique is not viable for mapping *in vivo*. The optical imaging of intrinsic signals allows simultaneous recording of neuronal activity over large areas of cortex^{6–9}. However, this technique cannot be considered to be noninvasive, and furthermore, its application is limited to the exposed cortical surface^{9,10}.

The progress of blood-oxygenation level-dependent functional magnetic resonance imaging^{11,12} raises hope that the functional architecture of the living brain can be visualized noninvasively, avoiding the limitations of the aforementioned techniques. Using the paramagnetic deoxyhemoglobin as an endogenous contrast agent^{11,12}, BOLD-based functional images can be obtained *in vivo* (in contrast to the 2-deoxyglucose (2-DG) technique^{5,13}), do not require extrinsic contrast agents (in contrast to the positron emission technique^{14,15}) and can access activation signals from the entire brain (in contrast to optical imaging^{6–9}). Most importantly, the noninvasiveness of MRI ideally suits this technique for studying the human brain during cognitive and perceptual tasks^{16–21}.

Numerous BOLD studies during cognitive¹⁶, motor¹⁷ and perceptual^{18–21} tasks indicate good spatial correlation between neuronal and hemodynamic responses at a coarse scale (several millimeter to centimeter), and the BOLD signal pointspread is comparable to that of optical imaging²¹. The ability of BOLD fMRI to map the columnar architecture of the brain, however, is controversial, as the ultimate functional specificity of BOLD is undetermined. Because optical spectroscopy data predicts a 'biphasic' BOLD response following neuronal stimulation^{22,23} (with each BOLD phase potentially yielding different mapping

resolutions), it becomes imperative to determine the limits of the functional specificity that can be achieved with BOLD. The exact temporal kinetics of the BOLD responses in mammalian brains, however, remain vigorously debated (compare refs. 24–26 with refs. 27, 28); thus it remains to be seen whether the functional specificity of BOLD is sufficient to map the basic computational units of the brain's functional architecture, namely, that of cortical columns.

RESULTS

To resolve the question of whether and to what extent the columnar architecture of the brain can be labeled using the BOLD-fMRI technique, we used ultra-high field magnets to obtain MR signals originating from individual orientation columns in cat visual cortex (area 18). Visual stimuli were optimized to drive orientation-selective, complex-type area 18 neurons²⁹. In this study, area 18 was used because the distance between two iso-orientation columns is greater in this area than in area 17 (ref. 30). Furthermore, area 18 on the lateral gyrus is essentially flat in the cat and can be covered by a single imaging slice. We carried out a total of ten semi-chronic experiments in ten hemispheres of five different animals. Unless otherwise mentioned, similar results were obtained in all ten experiments. Statistical data for all ten studies are given in parentheses.

Figure 1a shows an anatomical MR image of cat visual cortex on the lateral gyrus. All activation maps were derived from a plane tangential to area 18 on the lateral gyrus (green box, Fig. 1a). Colored pixels indicating regions of increased BOLD-signal change (Fig. 1c; see Methods) reveal the pattern of cortical activation in response to a moving grating oriented at 45°. As indicated in this panel, robust and homogenous activities were observed in the lateral gyri of both hemispheres. The region of activity extended several millimeters in anterior–posterior and medial–lateral directions.

In cat area 18, the average spacing between two neighboring iso-orientation columns is ~1.2–1.4 mm (ref. 30). Therefore, the nominal in-plane resolution of 156 × 156 μm² per pixel achieved in this study (see Methods) should have been sufficient to resolve individual orientation columns. As evident in Fig. 1c, however, a 'columnar' layout was not obtained. All four activation maps

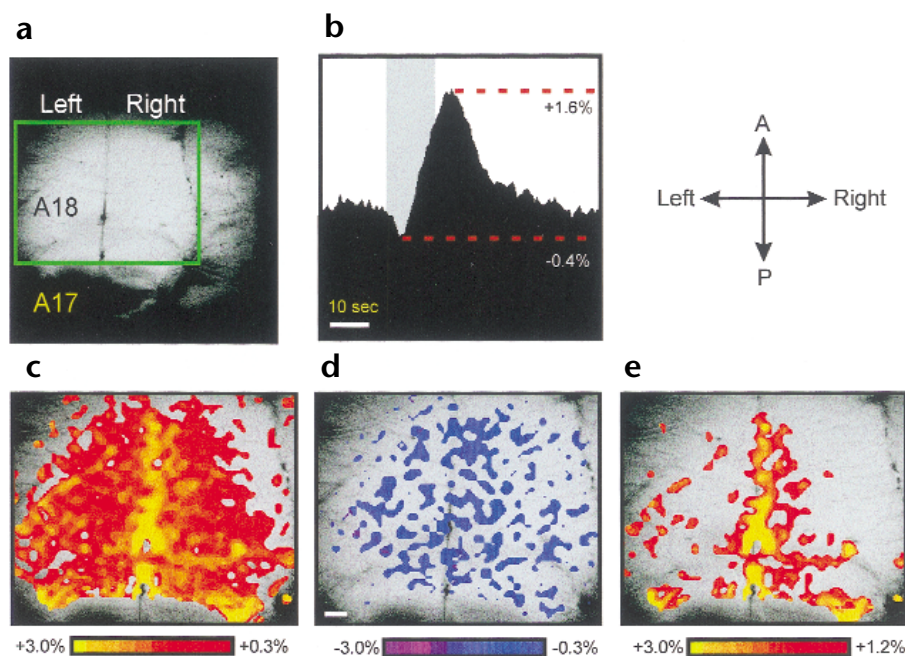


Fig. 1. Improvement of spatial specificity of BOLD using the initial negative signal changes. (a) Anatomical image of cat area 18 on the lateral gyrus (image size, $2 \times 2 \text{ cm}^2$). The green box indicates the position of the imaging slice used to obtain the activation maps displayed in this study. (b) The biphasic MR signal time course following visual stimulation. Stimulus duration of 10 s is marked by the gray box 'behind' the time course. Scale bar (b), 10 s. (c) Pattern of increased BOLD activity in response to moving 45° gratings. The positive BOLD percent changes are marked with colors as indicated by the color scale below. (d) Functional map for which only negative BOLD percent changes occurring within the first two seconds after stimulus onset were used. The color scale below indicates the negative percent changes. (e) The pattern of positive BOLD responses after the threshold for functional image construction was raised to match the number of the activated pixels to that in panel (d). See text for details. Scale bar (c–e), 1 mm. A, anterior; P, posterior.

obtained in response to moving gratings of four different orientations (0° , 45° , 90° , 135°) yielded homogeneous spatial distributions that were hardly distinguishable (data not shown; see also ref. 31).

This result is consistent with optical spectroscopy data^{22,23}, suggesting that the stimulation of cortical neurons gives rise to a biphasic hemodynamic response of which only the early increase of local deoxyhemoglobin (and hence a decrease in MR signal) reflects increased neuronal activity and oxygen consumption^{22,23}. Subsequent decrease of deoxyhemoglobin (and hence an increase of MR signal), which forms the basis for conventional BOLD^{11,12}, is hypothesized to originate mainly from the widespread increase in blood flow, thus making it less suitable to discriminate electrically active from inactive columns.

In cat visual cortex, the time evolution of MR signals was indeed biphasic (Fig. 1b). Following visual stimulation (as indicated by the gray box behind the time course), the MR signal decreased, reaching a minimum of about -0.2% to -0.4% ($-0.28 \pm 0.1\%$, $n = 10$) around 3 seconds ($2.9 \pm 0.7 \text{ s}$, $n = 10$) after the stimulus onset. The signal then reversed, yielding a maximum positive signal change of 1.0 – 2.0% ($1.3 \pm 0.4\%$, $n = 10$) approximately 8–10 seconds after stimulus onset ($8.0 \pm 1.3 \text{ s}$, $n = 10$). Biphasic BOLD responses following visual stimulation were observed in all ten experiments at two different magnetic fields.

As the early negative signal changes are likely to reflect the transient increase of local deoxyhemoglobin in parenchymal tissue^{22,23}, their use in generation of a functional map can be

expected to greatly enhance the functional specificity of fMRI. Such an improvement of functional specificity was achieved in our study (Fig. 1d). Here, only the 'negative' BOLD percent changes originating within the first two seconds after the stimulus onset were used to generate functional maps (see Methods). The colored pixels indicate regions of significant decrease in the MR signals following visual stimulation. In sharp contrast to the conventional fMRI maps based on the positive BOLD-signal changes (Fig. 1c), the foci of the negative signal changes are confined to patchy clusters (Fig. 1d). In line with the iso-orientation columns in cat detected with 2-DG³⁰ and optical imaging^{32,33} techniques, such semi-ellipsoidal and irregularly shaped clusters were broadly distributed over the approximated area 18 with an average periodicity of about $1.34 \pm 0.23 \text{ mm}$. Note also that the areas defined by negative signal changes were located largely in tissue areas, excluding regions of large blood vessels such as that surrounding the sagittal sinus.

Given the large difference in absolute amplitude between the negative and positive signal changes, it is conceivable that the differences in spatial pattern between the positive (Fig. 1c) and negative (Fig. 1d) maps could be simply due to the difficulty

in equating signal-threshold levels. Therefore, as a control, we raised the threshold for positive responses to match the number of activated pixels to that in the negative map (Fig. 1e). The resulting positive map largely reflects the pattern of surface vasculature in visual cortex.

Patterns of negative activity obtained from the same patch of cortex while the animal viewed four different orientation stimuli further corroborate functional significance of the negative BOLD signals (Fig. 2a–d). Analogous to 2-DG³⁰ and optical imaging^{32,33}, we show regions of high activity (large negative signals) as dark pixels. Each pattern of negative activity was highly specific to the respective stimulus orientation. To support this notion, outlines of the orientation patches for 90° and 135° maps were overlaid on the maps obtained for the respective orthogonal orientations (Fig. 2a–d).

It is clear from these panels that the patches for orthogonal orientations occupied cortical territories that were mostly complementary to each other. The complementarity between maps of orthogonal orientations was highly significant (linear correlation between 0° and 90° maps, $r = -0.4$, $p < 10^{-6}$; between 45° and 135° , $r = -0.55$, $p < 10^{-6}$; see Methods). Stimulus-selective responses based on negative BOLD signals were reflected at the columnar scale (Fig. 2e and f); these panels present the signal time courses obtained from 45° and 135° orientation columns (in green and in red, respectively; see Methods). MR signals in pixels representing 45° columns (green trace) decreased transiently during

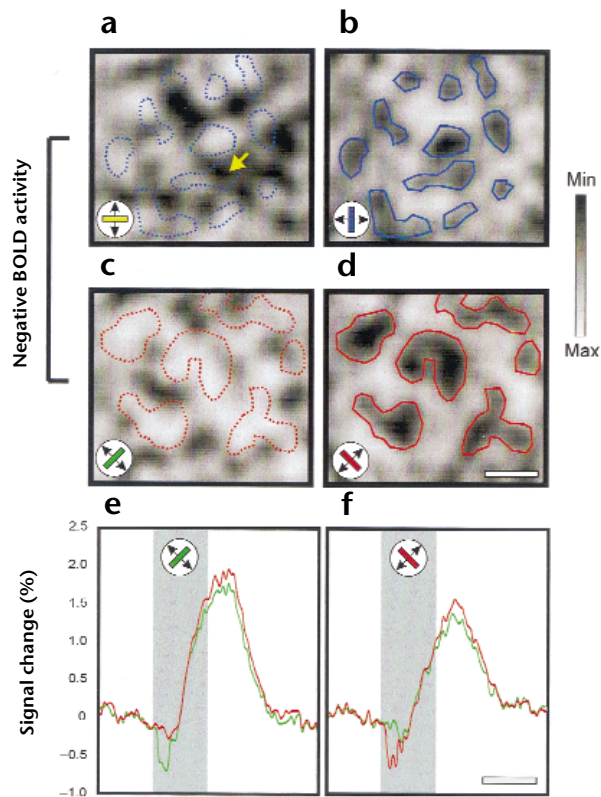


Fig. 2. Representation of orthogonal orientations in complementary cortical domains. (a–d) Patterns of negative activity in response to four orientations (0°, 45°, 90°, 135°). Regions of negative signal changes during the first two seconds following visual stimulation are displayed as dark pixels. For visual inspection of the complementarity between the orthogonal orientation maps, the patches in panels (b) and (d) are outlined (in blue and red, respectively) and overlaid on the maps in panels (a) and (c), respectively. With few exceptions (marked by yellow arrowheads), the maps for orthogonal orientations are complementary to each other. Scale bar, 1 mm. (e, f) The signal time courses for 45° (green) and 135° (red) columns during the stimulation with 45° (e) and 135° (d) orientation stimuli. The stimulation duration of ten seconds is marked by the gray boxes behind the time courses. Scale bar (e, f), 10 s.

45° stimulation (Fig. 2e), whereas little or no such decrease was observed during 135° stimulation (Fig. 2f). Likewise, MR signals from 135° columns (red trace) decreased transiently in response to the 135° stimulus (Fig. 2f), but not to the complementary 45° stimulus (Fig. 2e). The difference between 45° and 135° columns in magnitude of the early negative signals during the 45° (Fig. 2e) and 135° (Fig. 2f) stimulation was statistically significant ($p < 0.005$ and $p < 0.003$, respectively; paired t -test).

The positive BOLD signals (Fig. 2e and f), on the other hand, were much less suited to discriminate between 45° and 135° columns, as they yielded largely overlapping time courses for the two orthogonal stimuli. The differences in positive signals originating from the orthogonal columns were statistically insignificant ($p = 0.19$, paired t -test). To allow more direct comparison of the map quality, we also calculated the 45° and 135° maps obtained during the positive BOLD period (Fig. 3a and b). All functional maps depicted in Figs. 2 and 3 were acquired in the same fMRI studies, and images were processed with analogous methods (see Methods). In contrast

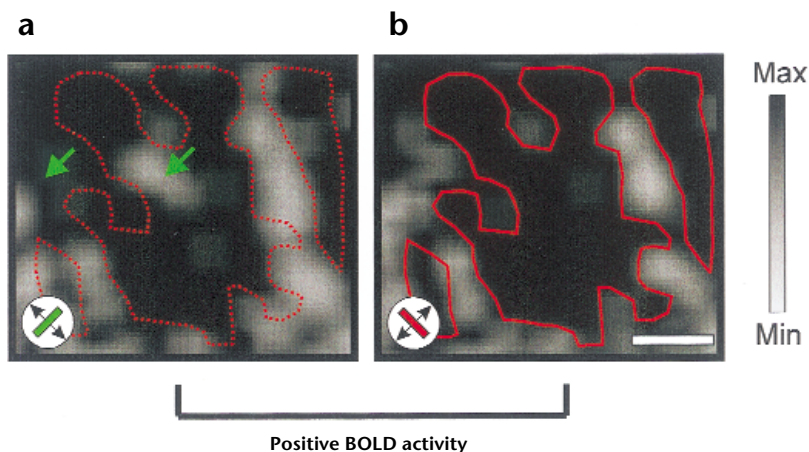
to the patchy, interdigitized columns of the negative maps, the domains of the positive BOLD responses were larger, with no apparent periodicity. The outlines of the 135° map from Fig. 3b were then overlaid on the 45° map (Fig. 3a). The regions of positive activity for the orthogonal orientations were mostly overlapping (linear correlation between the two maps, $r = 0.69$, $p < 10^{-6}$). The results in Figs. 2 and 3 indicate, therefore, that although the amplitudes of the negative signals were far smaller than those of the positive signals, the stimulus-specific contrast of the negative signals was superior to that of the positive signals. Based on Fig. 2e and f, the stimulus-specific contrast of the negative signals was calculated to be about 6.5 times larger than that of the positive signals.

The ultimate validation of the veracity of the iso-orientation columns based on negative BOLD changes would require simultaneous single-unit recording. Such simultaneous recording, however, would require placement of the recording electrodes in the iso-center of the magnetic bore, resulting in devastating magnetic field interferences. Furthermore, it would be almost impossible to change the electrode track or introduce new electrodes without repositioning the animal. Alternatively, the specificity of the negative BOLD signals at the columnar scale can be tested by comparing their detailed spatial pattern with that obtained by using more traditional brain-mapping techniques. A characteristic and invariant feature of the mammalian orientation system is the presence of ‘topological singularities’^{32–34}, which are observed in many species using both multi-electrode^{34,35} and optical-imaging^{32,33,36–38} techniques. Therefore, to validate the functional specificity of the negative BOLD maps, we calculated the ‘composite-angle’ maps through vector summation of the underlying activation maps obtained for the four different orientations (see Methods; Fig. 4).

In the composite map based on only the early negative BOLD signals (Fig. 4a), the colors (preferred orientations) change smoothly, forming a map of orientation selectivity. The continuity of orientation preferences is interrupted only at the singular points (termed orientation pinwheels) where the domains for all orientations converge, as observed using multi-electrode^{34,35} and optical imaging^{32,33,36–38} techniques. Each orientation is represented only once around such a pinwheel; therefore each of these topological singularities takes on one of two rotational chiralities, namely clockwise or counter-clockwise pinwheels. Two such pinwheels are enlarged (Fig. 4a, right). The pinwheel density and the ratio between clockwise and counter-clockwise singularities found in negative BOLD composite maps were in excellent agreement with those obtained with optical imaging. We found a pinwheel density of 1.46 ± 0.17 pinwheels per mm^2 ($n = 4$); in comparison, optical imaging studies^{32,37} yielded average pinwheel densities of 1.2–1.95 pinwheels per mm^2 . Likewise, the ratio of clockwise to counterclockwise pinwheels was found to be roughly 1:1 in both negative-BOLD (1:0.89, $n = 4$) and optical imaging³⁷ (1:0.9) data.

Although the above data are in excellent agreement with data from multi-electrode^{34,35} and optical imaging studies^{32,33,36–38}, it is theoretically possible but unlikely that such topological singularities could arise from a randomly distributed pattern of activity³⁹. Therefore, as a control, composite maps based on signals obtained before stimulus onset (Fig. 4b) and those during the delayed positive BOLD changes (Fig. 4c) were also calculated. All steps for composite-map construction were performed exactly as for Fig. 4a (see Methods). Unlike the composite map based on negative BOLD signals (Fig. 4a), the maps based on

Fig. 3. Representation of orthogonal orientations of positive BOLD maps. (a, b) Functional maps based on positive signal changes obtained with 45° and 135° stimuli, respectively. High positive signals are represented by dark pixels (see text). Maps in Figs. 2 and 3 were obtained from the same experiment. The domains of high activity in 135° map (b) are outlined and overlaid on the 45° map (a). Most of the active domains in both maps overlapped extensively, except a few areas as marked with green arrowheads. Scale bar, 1 mm.



control (Fig. 4b) or delayed positive BOLD signals (Fig. 4c) displayed none of the characteristic features of the mammalian angle maps.

DISCUSSION

Our results indicate that the functional specificity of BOLD at the columnar scale depends highly on the temporal dynamics of the underlying signals. If the early negative signals are used, functional maps at columnar resolution can be obtained without differential imaging (see below). The delayed positive BOLD changes, on the other hand, clearly indicated the pattern of the overall activation *per se* in the visual cortex, but were less suited to discriminate between active and inactive columns, as they were more diffuse^{21–23} and less specific to the individual stimulus properties.

It is, of course, conceivable that, in principle, even such diffuse positive BOLD signals might yield columnar patterns of activity if maps of orthogonal conditions were subtracted from each other. Such differential imaging had been suggested for analyzing optical imaging⁴⁰ and conventional (positive) BOLD data⁴¹. Although the use of a differential method for optical-imaging data might be defensible given the well established verification of intrinsic signals with extensive single-unit studies^{37,38},

the use of a differential method for BOLD fMRI data poses severe difficulties. In differential imaging, one activation map (for example, of the left eye) is subtracted from the other activation map (the right eye), with the assumption that the two maps yield complementary activation patterns. If this assumption is true—such as between left- and right-eye domains—then the result of the subtraction is tautological, because it was known in advance. However, if the assumption is not true or simply unknown, as for most receptive-field properties, then the subtraction method will probably give the wrong answer. Without direct validation of BOLD using simultaneous single-unit recordings, the applicability of the differential method for BOLD data remains questionable. The main significance of the ‘negative BOLD’ imaging is therefore that a columnar pattern of high functional specificity can be obtained directly, without the need for such differential methods.

As the T_2 and T_2^* -weighted BOLD contrast predominantly originates from the regional changes in paramagnetic deoxyhemoglobin concentration^{10,11,42}, the early decrease of BOLD signals can most likely be attributed to the regional increase of deoxyhemoglobin following neuronal stimulation. Although alternative explanations exist^{43,44}, the most parsimonious explanation for such transient BOLD signal decrease is caused by elevated oxygen consumption⁴⁴ in the active orientation column without a commensurate increase in blood flow^{22,23}.

Recently, similar decreases in BOLD signals have been observed in the visual cortices of awake human^{24–26,45} and anesthetized nonhuman primates⁴⁶ during perceptual

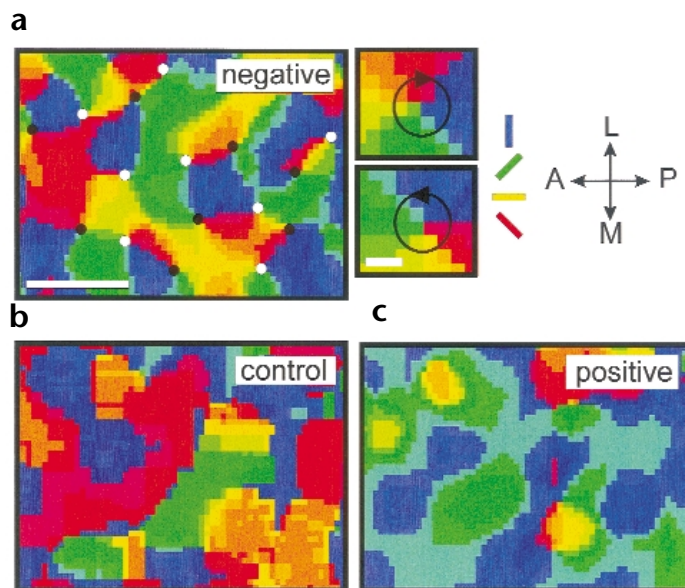


Fig. 4. fMRI-based composite angle maps. (a) The composite angle map obtained through pixel-by-pixel vector addition of the four single iso-orientation maps based on negative signal changes. The color key next to (a) was used for color coding the resulting orientation preferences. Overall continuity of the orientation preferences is interrupted at the orientation pinwheels where the cortical columns for different orientations are circularly arranged. The white and black circles in (a) depict clockwise and counterclockwise pinwheels, respectively. Two of such pinwheels are enlarged right (a). Scale bar for the enlarged pinwheels, 200 μm . As a control, the composite maps based on MR signals obtained before stimulus onset (b) and during positive BOLD signals (c) are also displayed. Maps in (b) and (c) were obtained from the same cortical region as in (a). The control maps are devoid of topological structures characteristic of genuine composite angle maps. Scale bar (a–c), 1 mm. A, anterior; P, posterior; M, medial; L, lateral.

tasks, indicating that the capability of BOLD-fMRI to label functional columns *in vivo* should also be applicable in humans and monkeys. We conclude from our study that noninvasive fMRI of brain functions can be performed at the columnar levels. Thus it now becomes possible to study the precise three-dimensional layouts of columnar structures in mature and developing brains, regardless of their location in the brain.

METHODS

Animal preparation. All animal experiments were performed with institutional approval. Animals were initially anesthetized with a ketamine (10–25 mg per kg, i.v.) and xylazine (2.5 mg per kg) cocktail. The animals were intubated and artificially ventilated (25–35 strokes per min, 15–30 ml per stroke) under isoflurane anesthesia (0.8–1.5%) in a N₂O:O₂ mixture of 70:30 throughout the experiment. The animal's eyes were refracted and corrective contact lenses used if necessary. The animal was placed in a cradle and restrained in normal postural position using a custom-designed stereotaxic frame. Endtidal CO₂, respiration rate and rectal temperature were monitored throughout the experiment. Following the three-to-five-hour MR experiments, gas anesthesia was discontinued, and animals were kept on the respirator until they could breathe independently. The animals were observed for 0.5–2.0 h before being returned to their littermates.

Stimulation protocol. Animals were stimulated binocularly. Visual stimuli consisted of high-contrast square-wave moving gratings (0.15 cycles per degree, 2 cycles per s) of four different orientations (0°, 45°, 90°, 135°), optimized to elicit responses from neurons in area 18 of the cat visual cortex²⁹. During the resting period, a stationary grating pattern of identical spatial frequency and orientation was presented. A video projector (Resonance Technology, Northridge, California; resolution, 640 × 480 pixels) was used to project the visual stimuli onto a screen positioned 15 cm from the animal's eyes. The screen covered about 37° of the animal's visual field.

MR methods. After placing the animal in a cradle, we placed a small surface coil (diameter, 1.2 cm) on top of the animal's head corresponding to the Horsley-Clark A3. All MR experiments were performed on an Oxford (4.7 T, 40 cm in diameter; Oxford, UK) or Magnex (9.4 T, 31 cm in diameter; Abingdon, UK) horizontal MRI scanner equipped with a magnetic field gradient of 15 or 30 gauss per cm, respectively. Data obtained at two magnetic field strengths were analyzed separately. The amplitude and phase of the biphasic time courses obtained at the two field strengths however, were averaged together, as they yielded comparable results. BOLD measurements on a single image slice was made using gradient-echo echo-planar imaging (EPI). The imaging slice was positioned ~500 μm below the pia to avoid superficial draining vessels. The MR imaging parameters were data matrix, 64 × 64; single-shot (4.7 T) or 2-shot (9.4 T) EPI; FOV, 2 cm × 2 cm; slice thickness, 2 mm; TE, 31 ms (4.7 T) or 12 (9.4 T) ms; TR, 0.5 s. A total of 160 images were acquired during each epoch (60 images before stimulation, 20 images during stimulation and 80 images after stimulation). Images with a 64 × 64 matrix were zero-filled to a 128 × 128 matrix, resulting in nominal in-plane resolution of 156 × 156 μm² per pixel. Images obtained for the same orientations within a single fMRI session were averaged for signal-to-noise ratio improvement (usually five to ten epochs).

Functional image construction. To determine the existence of BOLD activity *per se*, the MR signals were first cross-correlated with the stimulation protocol⁴⁷. The cross-correlation coefficient threshold was set at > 98% confidence level. The percent-change maps within the negative and positive portions of BOLD time course were averaged into respective time-binned maps ('positive' and 'negative' map, respectively). For the map of the negative response, individual pixels showing negative percent change ≥ 0.5–1.0 s.d. from the mean baseline percent change were taken as statistically significant. Because we used clustered pixel analysis with a cluster size of 4 pixels, the nominal *p*-value for our threshold was *p* < 0.2 (ref. 47). The same threshold was used for calculating the four different

iso-orientation maps for each experiment. For the positive response (Fig. 1c), the threshold was raised in proportion to ratio of the maximum positive to the minimum negative BOLD response for each animal (approximately fivefold). For the negative and positive BOLD maps depicted in Fig. 1, no subtraction or image filtering method was applied.

Analysis of iso-orientation maps. Similar image-processing methods were used to construct the iso-orientation maps based on negative or positive BOLD data. Analogous to the standard analysis of optical-imaging data^{32,33,37}, responses to the four different orientations were obtained by dividing each 'single orientation map' (raw percent-change maps) by the normalized sum of four orientations ('cocktail blank'). For displaying the maps, the dynamic range of the negative (Fig. 2a–d) and positive (Fig. 3a and b) maps were 'clipped' at the upper and lower three percent of the distribution and linearly mapped on an eight-bit gray scale. In both the negative and positive maps, high-frequency noise was removed using a 3 × 3 pixel Gaussian kernel. The complementarity of the orthogonal maps was tested by calculating the linear correlation coefficient between the two maps⁴⁸. Correlation coefficient *p*-values were calculated using standard algorithms⁴⁸. For the MR time courses in Fig. 2, the ROI for the 45° columns was selected on the basis of negative responses during only the 45° stimulation. The same ROI was then used to plot the time course of those pixels during the 135° stimulation. Likewise, the ROI for the 135° columns was selected on the basis of negative responses during only the 135° stimulation. This ROI was then used to plot the time course of the pixels during the 45° stimulation. The differences in positive signal contrasts during the 45° and 135° stimulations were therefore independent of the initial pixel selection process.

Analysis of angle maps. Composite angle maps for the negative BOLD changes (Fig. 4a) were obtained through a pixel-by-pixel vector addition of the four iso-orientation maps (see above) with the negative percent changes as vector amplitudes and the respective stimulus orientations as vector angles^{7,32,33}. Such composite angle maps were obtained for four different experiments that yielded the best contrast-to-noise ratio. The resulting angle at each pixel was color-coded using a circular color table. The positions and densities of the pinwheel centers were detected by calculating the spatial gradients of the composite angle map^{32,37} and checked visually. As a control, 'composite' maps were also calculated based on MR signals obtained before visual stimulation (Fig. 4b) and those obtained during delayed positive BOLD responses (Fig. 4c; 8–20 s after stimulus onset). For the sake of consistency, the composite maps in Fig. 4a–c were generated using identical methods for the region of interest, threshold and vector-summation.

ACKNOWLEDGEMENTS

We thank K. Ugurbil for continuing support of our project and S. Ogawa, A. Grinvald, R.B. Tootell, J. Ashe and A. P. Georgopoulos for suggestions and comments. H. Merkle and J. Strupp provided support in hardware and software. This work was supported by the NIH (NS38295, MH57180, NS10930, RR08079), the Minnesota Medical Foundation and the Keck Foundation.

RECEIVED 20 AUGUST; ACCEPTED 29 NOVEMBER 1999

1. Brodmann, K. *Vergleichende Lokalisationslehre der Grosshirnrinde* (Johann Ambrosius Barth, Leipzig, 1909).
2. Hubel, D. H. & Wiesel, T. N. Receptive field, binocular interactions and functional architecture in the cat's visual cortex. *J. Physiol. (Lond.)* **160**, 106–154 (1962).
3. LeVay, S., Stryker, M. P. & Shatz, C. J. Ocular dominance columns and their development in layer IV of cat's visual cortex. *J. Comp. Neurol.* **179**, 223–244 (1978).
4. LeVay, S. & Nelson, S. B. *Vision and Visual Dysfunction* 266–315 (Macmillan, Houndsmill, 1991).
5. Sokoloff, L. *et al.* The ¹⁴C-deoxyglucose method for the measurement of local cerebral glucose utilization: theory, procedure, and normal values in the conscious and anesthetized albino rat. *J. Neurochem.* **28**, 897–916 (1977).

6. Grinvald, A., Lieke, E., Frostig, R. D., Gilbert, C. D. & Wiesel, T. N. Functional architecture of cortex revealed by optical imaging of intrinsic signals. *Nature* **324**, 361–364 (1986).
7. Ts'o, D. Y., Frostig, R. D., Lieke, E. E. & Grinvald, A. Functional organization of primate visual cortex revealed by high resolution optical imaging. *Science* **249**, 417–420 (1990).
8. Frostig, R. D., Lieke, E. E., Ts'o, D. Y. & Grinvald, A. Cortical functional architecture and local coupling between neuronal activity and the microcirculation revealed by in vivo high-resolution optical imaging of intrinsic signals. *Proc. Natl. Acad. Sci. USA* **87**, 6082–6086 (1990).
9. Bonhoeffer, T. & Grinvald, A. The layout of iso-orientation domains in area 18 of cat visual cortex: optical imaging reveals a pinwheel-like organization. *J. Neurosci.* **13**, 4157–4180 (1993).
10. Stetter, M. & Obemayer, K. Simulation of scanning laser technique for optical imaging of blood-related intrinsic signals. *J. Opt. Soc. Am. A* **16**, 58–70 (1999).
11. Ogawa, S. *et al.* Intrinsic signal changes accompanying sensory stimulation: functional brain mapping with magnetic resonance imaging. *Proc. Natl. Acad. Sci. USA* **89**, 5951–5955 (1992).
12. Kwong, K. K. *et al.* Dynamic magnetic resonance imaging of human brain activity during primary sensory stimulation. *Proc. Natl. Acad. Sci. USA* **89**, 5675–5679 (1992).
13. Loewel, S. & Singer, W. Tangential intracortical pathways and the development of iso-orientation bands in cat striate cortex. *Dev. Brain Res.* **56**, 99–115 (1990).
14. Fox, P. T. & Raichle, M. E. Focal physiological uncoupling of cerebral blood flow and oxidative metabolism during somatosensory stimulation in human subjects. *Proc. Natl. Acad. Sci. USA* **83**, 1140–1144 (1986).
15. Posner, M. I. & Raichle, M. E. *Images of Mind* (Freeman, New York, 1994).
16. Wagner, A. D. *et al.* Building memories: remembering and forgetting of verbal experiences as predicted by brain activity. *Science* **281**, 1188–1191 (1998).
17. Kim, S.-G. *et al.* Functional magnetic resonance imaging of motor cortex: hemispheric asymmetry and handedness. *Science* **261**, 615–617 (1993).
18. DeYoe, E. A. *et al.* Mapping striate and extrastriate visual areas in human cerebral cortex. *Proc. Natl. Acad. Sci. USA* **93**, 2382–2386 (1996).
19. Sereno, M. I. *et al.* Borders of multiple visual areas in humans revealed by functional magnetic resonance imaging. *Science* **268**, 889–893 (1995).
20. Tootell, R. B. *et al.* Functional analysis of V3A and related areas in monkey visual cortex. *J. Neurosci.* **17**, 7070–7078 (1997).
21. Engel, A. S., Glover, G. H. & Wandell, B. A. Retinotopic organization in human visual cortex and the spatial precision of functional MRI. *Cereb. Cortex* **7**, 181–192 (1997).
22. Malonek, D. & Grinvald, A. Interactions between electrical activity and cortical microcirculation revealed by imaging spectroscopy: Implication for functional brain mapping. *Science* **272**, 551–554 (1996).
23. Malonek, D. *et al.* Vascular imprints of neuronal activity: relationships between the dynamics of cortical blood flow, oxygenation, and volume changes following sensory stimulation. *Proc. Natl. Acad. Sci. USA* **94**, 14826–14831 (1997).
24. Ernst, T. & Henning, J. Observation of a fast response in functional MR. *Magn. Reson. Med.* **32**, 146–149 (1994).
25. Menon, R. S. *et al.* BOLD based functional MRI at 4 Tesla includes a capillary bed contribution: Echo planar imaging correlates with previous optical imaging using intrinsic signals. *Magn. Reson. Med.* **33**, 453–459 (1995).
26. Hu, X., Le, T. H. & Ugurbil, K. Evaluation of the early response in fMRI in individual subjects using short stimulus duration. *Magn. Reson. Med.* **37**, 877–884 (1997).
27. Marota, J. J. A. *et al.* Investigation of the early response to rat forepaw stimulation. *Magn. Reson. Med.* **41**, 247–252 (1999).
28. Silva, A. C., Lee, S.-P., Iadecola, C. & Kim, S.-G. Early characteristics of CBF and deoxyhemoglobin changes during somatosensory stimulation. *J. Cereb. Blood Flow Metab.* **20**, 201–206 (2000).
29. Movshon, J. A., Thompson, I. D. & Tolhurst, D. J. Spatial and temporal contrast sensitivity of neurons in areas 17 and 18 of the cat's visual cortex. *J. Physiol. (Lond.)* **283**, 101–120 (1978).
30. Loewel, S., Freeman, B. & Singer, W. Topographic organization of the orientation column system in large, flat-mounts of the cat visual cortex: A 2-deoxyglucose study. *J. Comp. Neurol.* **255**, 401–415 (1987).
31. Jezzard, P., Rauschecker, J. P. & Malonek, D. An *in vivo* model for functional MRI in cat visual cortex. *Magn. Reson. Med.* **38**, 699–705 (1997).
32. Bonhoeffer, T. & Grinvald, A. Iso-orientation domains in cat visual cortex are arranged in pinwheel-like pattern. *Nature* **353**, 429–432 (1991).
33. Kim, D.-S. & Bonhoeffer, T. Reverse occlusion leads to a precise restoration of orientation preference maps in visual cortex. *Nature* **370**, 370–372 (1994).
34. Swindale, N. W., Matsubara, J. A. & Cynader, M. S. Surface organization of orientation and direction selectivity in cat area 18. *J. Neurosci.* **7**, 1414–1427 (1987).
35. Diao, Y. C., Jia, W. G., Swindale, N. V. & Cynader, M. S. Functional organization of the cortical 17 per 18 border region in the cat. *Exp. Brain Res.* **79**, 271–282 (1990).
36. Maldonado, P. E., Goedecke, I., Gray, C. M. & Bonhoeffer, T. Orientation selectivity in pinwheel centers in cat visual cortex. *Science* **276**, 1551–1555 (1997).
37. Shmuel, A. & Grinvald, A. Functional organization for direction of motion and its relationship to orientation maps in cat area 18. *J. Neurosci.* **16**, 6945–6964 (1996).
38. Crair, M. C., Gillespie, D. C. & Stryker, M. P. The role of visual experience in the development of columns in cat visual cortex. *Science* **279**, 566–570 (1998).
39. Rojer, A. S. & Schwartz, E. L. Cat and monkey cortical columnar patterns modeled by bandpass-filtered 2D white noise. *Biol. Cybern.* **62**, 381–391 (1990).
40. Blasdel, G. G. Differential imaging of ocular dominance and orientation selectivity in monkey striate cortex. *J. Neurosci.* **12**, 3115–3138 (1992).
41. Menon, R. S., Ogawa, S., Strupp, J. P. & Ugurbil, K. Ocular dominance in human V1 demonstrated by functional magnetic resonance imaging. *J. Neurophysiol.* **77**, 2780–2787 (1997).
42. Ogawa, S., Menon, R. S., Kim, S.-G. & Ugurbil, K. On the characteristics of functional magnetic resonance imaging of the brain. *Annu. Rev. Biophys. Biomol. Struct.* **27**, 447–474 (1998).
43. Janz, C., Speck, O. & Henning, J. Time-resolved measurements of brain activation after a short visual stimulus: new results on the physiological mechanisms of the cortical response. *NMR Biomed.* **10**, 222–229 (1997).
44. Vanzetta, I. & Grinvald, A. Increased cortical oxidative metabolism due to sensory stimulation: implications for functional brain imaging. *Science* **286**, 1555–1558 (1999).
45. Yacoub, E. & Hu, X. Detection of the early negative response in fMRI at 1.5 Tesla. *Magn. Reson. Med.* **41**, 1088–1092 (1999).
46. Logothetis, N. K., Guggenberger, H., Peled, S. & Pauls, J. Functional imaging of the monkey brain. *Nat. Neurosci.* **2**, 555–562 (1999).
47. Forman, S. D. *et al.* Improved assessment of significant activation in functional magnetic resonance imaging (fMRI): use of a cluster-size threshold. *Magn. Reson. Med.* **33**, 636–647 (1995).
48. Press, W. H., Teukolsky, S. A., Vetterling, W. T. & Flannery, B.P. *Numerical Recipes in C* (Cambridge, UK, 1992).